Int J Thermophys (2007) 28:2076–2086
DOI 10.1007/s10765-007-0309-5

SSE- and Noise-Optimized InGaAs Radiation Thermometer

H. W. Yoon · C. E. Gibson · V. Khromchenko · G. P. Eppeldauer

Published online: 6 November 2007

Abstract For measurements of radiance temperatures in the range from 150°C to 1,000°C, low uncertainties in the temperature measurements can be achieved by using near-infrared InGaAs radiation thermometers. The design and construction of the NIST near-infrared radiation thermometer (NIRT) that is optimized for low size-of-source effect (SSE) and noise-equivalent temperatures are described. The NIRT utilizes a 50 mm diameter achromatic objective lens with low scatter that images a 4.5 mm diameter spot at a distance of 50 cm from the objective in an on-axis design. A Lyot stop is implemented in the design with the aperture stop placed after the field stop resulting in a collection f/12. A 3 mm diameter InGaAs detector is cooled to −70°C using a four-stage thermoelectric cooler to obtain high-shunt resistance for linear, low-noise operation at high transimpedance amplifier gains. For thermal and structural stability, the optical components are placed on four, 15 mm diameter graphite-epoxy rods making the optical throughput stable. Optical ray tracing with a commercial program is used to determine the Strehl ratio and other imaging parameters. A possible approach for a detector-based temperature scale in this range which could result in 10 mK ($k = 2$) thermodynamic temperature uncertainties at the In-point is discussed.

Keywords ITS-90 · Near-infrared radiation thermometer · Noise-equivalent temperature difference · Radiance temperature · Size-of-source effect · Thermodynamic temperature

H. W. Yoon (✉) · C. E. Gibson · V. Khromchenko · G. P. Eppeldauer
Optical Technology Division (844), National Institute of Standards and Technology, 100 Bureau Drive, Stop 8441, Gaithersburg, MD 29899-8441, USA
e-mail: howard.yoon@nist.gov

1 Introduction

Accurate determinations of radiance temperatures from 150°C to 1,000°C are important for the calibration of radiation thermometers, which are used in turn for process control or to transfer the calibration to other radiation thermometers. In this temperature range, one can establish a scale on radiation thermometers from the International Temperature Scale of 1990 (ITS-90) either by using the ITS-90 fixed-point blackbodies (FPBBs) from the In-point to the Ag-point with an interpolation equation or by using a variable-temperature blackbody (VTBB), whose temperatures are determined by contact, platinum resistance thermometers (PRT) [1]. In both approaches, the FPBB or the VTBB emissivity has to be measured or modeled so that the lowest uncertainties in the transfer to the radiation thermometer can be achieved. International comparisons of scales in this temperature range have revealed that the lowest uncertainties in radiance temperatures can be achieved using the fixed-point interpolation technique instead of using a VTBB [2]. Uncertainties from the use of FPBBs are possibly lower, since the temperatures are well-known and high spatial temperature uniformity of the cavity results in a high-emissivity blackbody. Variable-temperature blackbodies are expected to have larger uncertainties arising from difficulties in achieving uniform temperature distributions within the cavity and the differences in temperature between the contact thermometer and that of the radiating surface of the blackbody, thus resulting in larger uncertainties in the emissivity of the blackbody.

Although the method of calibrations using fixed-points is well established, commercial radiation thermometers which are temporally stable and able to view the small cavity openings of the FPBBs are not readily available. Furthermore, custom InGaAs radiation thermometers constructed by the national measurement institutes have conflicting designs [3,4]. Although reduction of the size-of-source effect (SSE) is a critical design feature due to the need to compare small-area fixed point blackbody cavities to large VTBB openings, implementation of the Lyot stop has been lacking. Furthermore, in the past, methods to decrease the noise-equivalent current of the radiation thermometer have not been extensively explored.

In this article, we describe a generalized design for an InGaAs-based radiation thermometer (RT) capable of measurements from the In-point to the Ag-point. The radiation thermometer also incorporates a Lyot stop, while utilizing a low-scatter objective lens. The construction utilizes carbon-epoxy rods for structural stability with temporal stability of the responsivity increased by the use of a room temperature-stabilized filter and cooled detector. The detector is contained in a hermetically sealed package to decrease the detector temperature below ambient temperatures in order to increase the shunt resistance for low-noise operations. It is hoped that instrumental designs discussed in this article can be adopted in future radiation thermometer designs to improve the performance of transfer standard radiation thermometers.

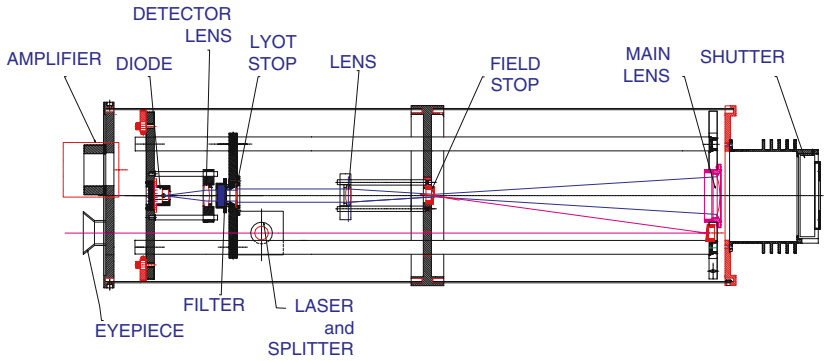

Fig. 1 Schematic of the InGaAs-based radiation thermometer with the optical components labeled. Outer diameter of the main body is 20.3 cm with a total length of 75 cm, excluding the front baffle. For alignment, the eyepiece is used to view the image on the tilted field stop. A laser can be made incident on the field stop for additional alignment

2 Radiation Thermometer Characterization

2.1 Physical Design

The schematic of the radiation thermometer is shown in Fig. 1. The internal elements are mounted on four 15 mm diameter graphite-epoxy rods for structural stability. The graphite-epoxy rods have a coefficient of thermal expansion (CTE) of $-0.5\times10^{-6}\,\mathrm{K}^{-1}$ that is smaller than that of fused silica [5]. The rods are attached to the front plate holding the objective lens, and the various separations between the optical elements can be smoothly adjusted by sliding along the through rods. The angled field stop is constructed from polished stainless steel with a beveled 3 mm diameter hole. The field stop is angled to reduce the back reflection of the image onto the objective lens, thus reducing the SSE. The specular reflection from the field stop is directed to a flat mirror for viewing through the telescope objective. The radiation through the field stop is collimated by the 70 mm focal length achromat and the plane of the objective lens is focused onto the Lyot stop. The presence of the Lyot stop is critical in reducing the SSE. The room temperature stabilized interference filter is constructed using hard, ion-assisted deposited layers at a center wavelength of 1,550 nm. The full-width at half-maximum bandpass of the filter is 100 nm. Due to the four-stage thermoelectric (TE) cooler, which limits the maximum size of the regular InGaAs detector, a 3 mm diameter detector is used. The detector lens focuses the 3 mm diameter object at the field stop onto a 1.5 mm diameter region on the detector, leading to an under-filled detector.

The outer case of the radiation thermometer is floating with respect to the optical elements attached to the graphite rods and is only fixed at the middle supporting plate. The case is constructed using 1.83 mm thick anodized aluminum tubing. The use of the Al tube facilitates rapid thermal equilibration between the laboratory temperature and the internal temperatures. Additionally, the heat-sink plate for the InGaAs detector is

Table 1 Design parameters of the InGaAs radiation thermometer (RT)

Object distance	50 cm
Image distance	33.3 cm
Objective focal length	20 cm
Field stop diameter	3.0 mm
Target diameter	4.5 mm
f/#	12
Lyot stop diameter	8 mm
Detector type	InGaAs
Detector diameter	3 mm
Detector temperature	−70°C
Filter center wavelength	1,550 nm
Filter FWHM bandpass	100 nm
Filter temperature	22°C
Collimator lens focal length	70 mm
Detector lens focal length	35 mm
Image diameter on detector	1.5 mm
RT diameter	20.3 cm
RT length	76.2 cm

thermally connected to the external tubing with copper-braided contacts which work to dissipate the heat generated from the use of the TE cooler. We are able to achieve −70°C with only passive cooling. Additional information on the construction of the radiation thermometer is given in Table 1.

2.2 Detector Optimization

The most important aspect of the radiation thermometer design is the selection of the detector to be used in the radiation thermometer. Due to the linearity and the wavelength region of the spectral power responsivity, a regular InGaAs diode was chosen. Since the small target diameter and the f/# limits the throughput of the RT, the preamplifier should have a dynamic range from $10^{10}\,\mathrm{V{\cdot}A^{-1}}$ to $10^{5}\,\mathrm{V{\cdot}A^{-1}}$ for measurements of blackbodies from the In-point to the Ag-point. In a transimpedance amplifier circuit, the shunt resistance of the input diode should have a value greater or equal to the feedback resistance for linear, low-noise amplification of the current. The measurement of the shunt resistances of both 1 mm diameter and 3 mm diameter InGaAs diodes in Fig. 2 shows that the shunt resistances have a semi-logarithmic relationship to temperature. The shunt resistances also increase as a linear function of the detector area, as expected for defects with a uniform surface density. Figure 2 shows that for 1 mm diameter diodes, shunt resistances greater than $10^{10}\,\Omega$ are achieved at detector temperatures of −20°C, which is possible with two-stage TE cooling. For 3 mm diameter diodes, detector temperatures of at least −40°C are needed to achieve value greater than $10^{10}\,\Omega$ shunt resistance. Unless the diode material quality is improved, larger diodes are expected to require greater cooling to obtain the same shunt resistances.

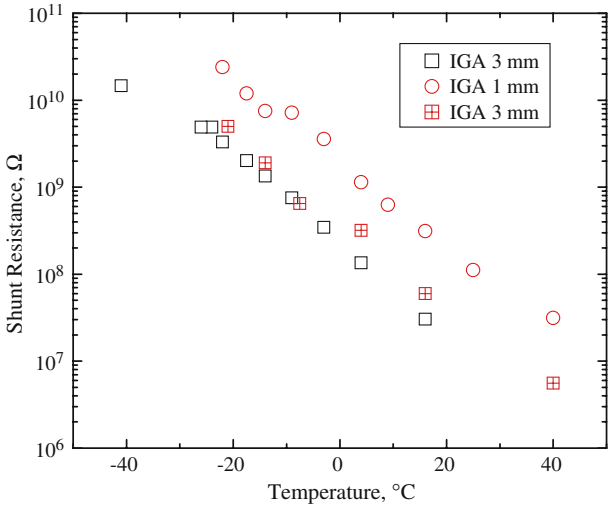

Fig. 2 Temperature-dependent shunt resistances of 1 and 3 mm diameter InGaAs (IGA) diodes. Shunt resistance of the diode should be comparable to the feedback resistance of the preamplifier circuit for low noise, linear operation

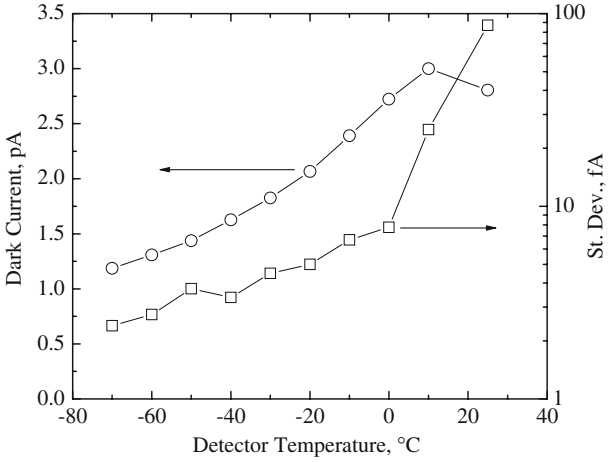

Fig. 3 Dark current (left axis) and standard deviation (right axis) of the dark current measured with a bandwidth of 0.3 Hz as a function of the 3 mm diameter InGaAs detector temperature. Standard deviation of the dark current of the InGaAs detector at −70°C nearly approaches Si-type detector performance

2.3 Temperature-Dependent Detector Performance

The importance of the ability to cool the detector to below ambient temperature is shown in Fig. 3. The dark current and the standard deviation of the dark current at a preamplifier gain of $10^{10}\,\mathrm{V{\cdot}A^{-1}}$ are shown. The standard deviations are measured using 10 measurements with the number of power-line cycles (NPLC) equal to 10, or 0.13 Hz. The dark current is weakly dependent on the detector temperature, with a

decrease from 3 pA to about 1 pA as the detector is cooled from room temperature to −70°C. The change in the dark current with decreasing temperature indicates that stabilizing the detector temperature is important in avoiding dark-current drift, especially at the In point where the net photocurrent is only about 23 pA. With cooling of the detector, the standard deviation of the dark current changes much more, from about 100 to 2.4 fA. Although the detector was cooled to lower temperatures than −70°C, the heat generated from the TE coolers could not be readily dissipated which lead to self-heating of the detector. We observed a slow drift of the dark current when the temperature of the detector was set to lower temperatures that precluded stable measurements of standard deviations of the dark current. These measurements indicate that close to Si-type performance of a few fA noise-equivalent current [6] is possible with four-stage TE cooling. This low-noise performance is especially important at the In-point, where any decrease in the noise-equivalent power directly leads to a decrease in the noise-equivalent temperatures.

2.4 Size-of-Source Effect

Since the radiation thermometer is designed to transfer ITS-90 temperatures to other blackbodies, the suppression of the SSE in comparing small fixed-point cavities to larger area variable temperature blackbody cavities are critical. In the design of a radiation thermometer to have a small SSE, it is important to use a low-scatter objective lens in addition to the incorporation of a Lyot stop [7]. Although the SSE can be changed by removing the objective lens, such drastic steps will result in a decrease of the entrance pupil, leading to extremely low throughput and inability to measure at low temperatures due to the high noise. Furthermore, the introduction of any element which can lead to further scatter into the field stop should be discouraged, such as protective windows or viewing beamsplitters, which are directly in the optical path of the radiation. The SSE is plotted in Fig. 4 using

$$\sigma\,(d, d_{\mathrm{o}}) = \frac{v(L, d) - v(L, d_{\mathrm{o}})}{v(L)}, \tag{1}$$

where d is the diameter of the uniform radiance source, d_{o} is the diameter of the central obscuration, and L is the radiance of the source. The signal measured while viewing the unobstructed radiance source is $v(L)$, and the signal measured while viewing the central obscuration with the diameter of the radiance source, d, is $v(L, d)$. The signal measured with the diameter of the variable aperture at the diameter of the central obscuration, d_{o}, is $v(L, d_{\mathrm{o}})$. The SSE measured using a 10 mm diameter central obscuration is shown in Fig. 4. The measurements are performed using a high-power, 1 W light-emitting diode (LED) source, as described previously [8]. The LED source has sufficient output in the near-infrared-wavelength region for these measurements. The low SSE measured at 50 mm source diameter indicates that our design is effective at suppressing internal scatter. The comparison of the SSE in terms of temperature corrections is shown in Table 2, with SSE values of 7×10^{-5} and 1×10^{-3} converted to their corresponding temperature corrections at the respective fixed points. The SSE

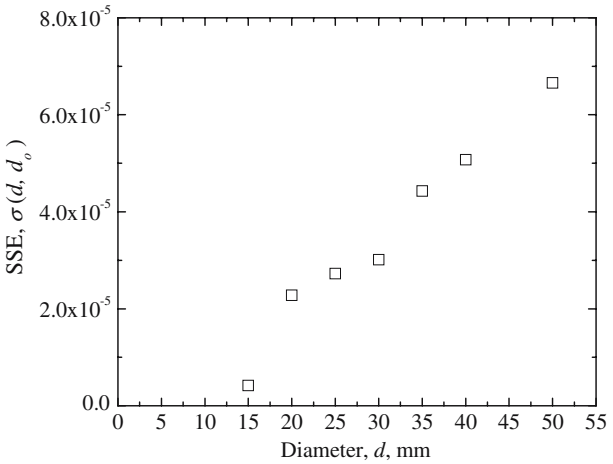

Fig. 4 SSE measured using a central obscuration, $d_o = 10$ mm, with the outer diameter, d, varied from 15 mm to 50 mm. Use of a low scatter objective, a tilted field stop, and a Lyot stop results in low SSE

Table 2 Size-of-source effect (SSE) at SSE $= 7 \times 10^{-5}$ and 1×10^{-3} converted to temperature corrections. The smaller SSE corrections can be folded into the uncertainty budget while the larger SSE requires a correction factor

Fixed point	Temperature (°C)	SSE $= 7 \times 10^{-5}$ (K)	SSE $= 1 \times 10^{-3}$ (K)
In	156.5985	0.001	0.020
Sn	231.928	0.002	0.027
Zn	419.527	0.004	0.052
Al	660.323	0.007	0.094
Ag	961.78	0.011	0.164

conversion to equivalent temperatures can be found from the derivative of the Wien approximation to Planck's radiance law,

$$\frac{\Delta L}{L} = \frac{c_2}{\lambda}\frac{\Delta T}{T^2}, \tag{2}$$

which shows the relationship between the uncertainty in radiance, L, to the uncertainty in blackbody temperature, T, where c_2 is the second radiation constant and λ is the wavelength. If the SSE can be reduced to 7×10^{-5}, then the corrections can be included as terms in the total uncertainty budget, while larger SSE values require systematic correction terms as shown in Table 2.

2.5 Optical Performance

The InGaAs radiation thermometer utilizes a commercial 50-mm-diameter achromat with a focal length of 200 mm with nearly 1:1 finite-conjugate imaging. Since commercial achromatic lenses are designed for infinite-conjugate imaging, the imaging

Table 3 Optical parameters of the 200 mm focal length achromatic objective lens. Moving the object distance at 1,550 nm by 25 mm results in comparable image distance to the 500 nm wavelength. Strehl ratio also improves at 1,550 nm as compared to 500 nm indicating better imaging performance

Wavelength (nm)	Object distance (mm)	Image distance (mm)	Strehl ratio
500	500	323.91	0.0738
1,550	500	334.49	0.213
1,550	525	324	0.238

performance suffers as shown by the Strehl ratio in Table 3. The Strehl ratio for perfect point source imaging will be 1.0, and the ratio will approach this value as the imaging performance improves. The Strehl ratio increases as the wavelength increases, indicating that imaging performance is better at 1,550 nm than at 500 nm. Furthermore, achromatic lenses will generally have two wavelengths where the image distances will be equal for a set object distance with the chromatic focal shift depending on the lens material and thickness. Since the radiation thermometer is designed to transfer a temperature scale from one blackbody to another without any desired spatial structure within the cavity, the need for imaging performance is much reduced. Although a single achromat will have much worse imaging performance than that of multi-element photographic-type lenses, the single, cemented achromat will have reduced scatter and consequently much lower SSE than that of multi-element lenses. All these optical performance metrics can be modeled using a commercial modeling program. Table 3 shows that although the alignment of the radiation thermometer can be performed in the visible wavelength, the object distances at 1,550 and 500 nm differ by 25 mm for the same image distance. Since the internal focus is difficult to adjust, the object distance can be offset by this difference to account for chromatic aberrations.

2.6 Preamplifier Gain Corrections

Since the InGaAs radiation thermometer should have a linear signal versus radiance of the blackbody, the preamplifier gain settings need to be normalized to one another. In this radiation thermometer, precision, metal-film-on-ceramic resistors are used in the transimpedance amplifier. The resistors are chosen to have a low-temperature variation of resistance. The preamplifier is attached to a Si detector with high shunt resistance and placed in front of a broadband white LED source. The 1 W, high-power LED source is chosen for its temporally stable output so that the gain ratios can be determined with low uncertainty. The optical power of the LED source incident on the detector is varied by using a combination of diffusers, variable source apertures, and by changing the distance between the source and the detector. The LED source, for the most stable operations, is left on for about 24 h to reach thermal equilibrium. The ratios of gain factors shown in Table 4 indicate that, at the lower gain settings, the ratios between two gains different by an order of magnitude are within the uncertainties of the measurements and the resistances. The greatest deviation is present at gain factors of 10^{10} and 10^{9} $V \cdot A^{-1}$ where the resistors used in the preamplifier deviate more from their assigned values.

Table 4 Gain ratios of the preamplifier measured using a 1 W white LED source with a Si detector

Gains compared	Gain ratios	Measurement uncertainty ($k = 2$)
$10^6/10^5$	9.998	0.002
$10^7/10^6$	10.001	0.002
$10^8/10^7$	10.000	0.002
$10^9/10^8$	10.000	0.002
$10^{10}/10^9$	9.957	0.002

Table 5 Gains and photocurrents at the fixed-point temperatures measured using a variable-temperature blackbody set at the respective temperatures. Standard deviations of the photocurrents at the respective temperatures are converted to noise-equivalent temperature differences (NETD)

Fixed point	Temperature (°C)	Gain ($V \cdot A^{-1}$)	Signal (A)	NETD (°C)
In	156.5985	10^{10}	2.26251×10^{-11}	0.0050
Sn	231.928	10^9	5.36748×10^{-10}	0.0011
Zn	419.527	10^7	7.45110×10^{-8}	0.0015
Al	660.323	10^6	2.23358×10^{-6}	0.0009
Ag	961.78	10^5	2.63766×10^{-5}	0.0013

3 Blackbody Measurements

The InGaAs radiation thermometer was placed in front of a VTBB that was set at the respective ITS-90 fixed-point temperatures. The measurements on actual fixed points could not be performed in time for this submission. These measurements are used to determine the gain settings of the preamplifier, the throughput of the radiation thermometer, and to measure the noise-equivalent temperature difference (NETD) at the fixed-point temperatures. Work is planned to measure the freezing points directly using the InGaAs radiation thermometer. The standard deviation of the signals at a particular set temperature is converted to NETD by using Eq. 2. The measured NETD could be affected by the temporal stability of the VTBB, and our measurements shown in Table 5 and plotted in Fig. 5 give the upper value of this parameter. The photocurrent at the In-point is comparable to that from the InGaAs radiation thermometers developed at other national measurement institutes, indicating that the throughputs are comparable. The lower NETD exhibited by the NIST design is due to the optimization of the preamplifier and detector, especially by four-stage cooling of the detector and the resultant decrease in the noise-equivalent photocurrent seen in Fig. 3. Once the NIST InGaAs radiation thermometer is calibrated using the ITS-90 fixed points, a modified three-parameter Planck version of the Sakuma-Hattori equation will be used for the interpolation.

We have also tried to use alternating-current (AC) mode measurements using a 10.1 Hz tuning-fork chopper placed directly in front of the field stop with a lock-in detection system. With the AC mode, lower blackbody temperatures, to 80°C, could be measured, although with the added complexities of using the lock-in amplifier. Further work is necessary to lower the uncertainties of AC-mode measurements.

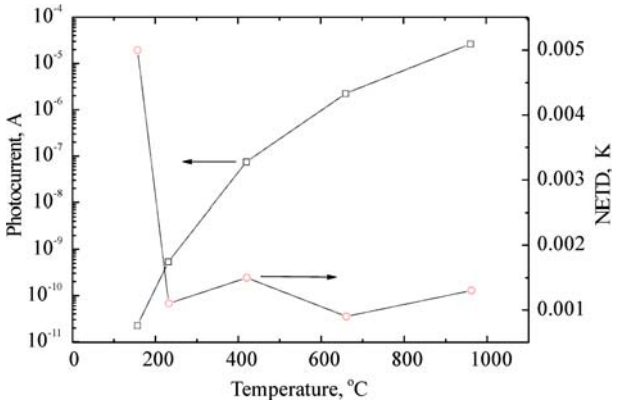

Fig. 5 Measured photocurrents of the InGaAs radiation thermometer at the various fixed-point temperatures. For convenience, measurements were performed using a variable-temperature blackbody set to the ITS-90 temperatures. The NETD was determined from the standard deviation of the measurements

4 Discussion and Future Work

Thus far, radiation thermometers with InGaAs detectors have only been used to transfer the source-based ITS-90 scale to other sources or blackbodies. Due to the developments of laser-based calibration facilities and the low-noise and high linearities of InGaAs detectors, the possibility of detector-based thermodynamic temperature determinations are being explored. The detector-based calibration of the InGaAs radiation thermometer would be performed in a similar manner as for a Si-diode based radiation thermometer [9]. A transfer radiometer would need to be calibrated for spectral power responsivity by comparison to the cryogenic, electrical-substitution radiometer using infrared lasers, and thus the optical power scale would be derived from the electrical power. The transfer radiometer would need a precision aperture and known spatial uniformity of responsivity so that the power responsivity can be converted to spectral irradiance responsivity. The conversion to irradiance responsivity can be performed with detectors in a trap configuration or with detectors that are attached to integrating sphere inputs. By combining a laser-irradiated sphere with the calibrated transfer radiometer, the InGaAs radiation thermometer can be calibrated for absolute detector-based radiance responsivity. Since Spectralon[1] and other sintered or packed polytetrafluoroethylene (PTFE) materials have a high reflectance at 1.55μm, integrating spheres have high throughput and spatial uniformity. It is anticipated that such a detector-based radiation thermometer could be calibrated to 0.05% ($k = 2$) [10]. The resulting thermodynamic temperature uncertainties are shown in Table 6.

[1] Certain commercial equipment, instruments, or materials are identified in this article to foster understanding. Such identification does not imply recommendation or endorsement by the National Institute of Standards and Technology, nor does it imply that the material or equipment are necessarily the best available for the purpose.

Table 6 Thermodynamic temperature uncertainties for a total uncertainty of 0.05% ($k = 2$) at the respective fixed-point temperatures

Fixed point	Temperature (°C)	Total Uncertainty = 0.05% ($k = 2$) (K)
In	156.5985	0.0099
Sn	231.928	0.0137
Zn	419.527	0.0258
Al	660.323	0.0469
Ag	961.78	0.0821

5 Conclusions

We described a noise-optimized InGaAs radiation thermometer operating at 1,550 nm that is capable of smaller than 5 mK NETD at 157°C. The SSE has also been reduced to less than 7×10^{-5} at 50 mm which leads to low uncertainties when comparing fixed-point blackbodies to other larger-area variable-temperature blackbodies. These results are due to the implementation of four-stage cooling of the diode, resulting in high shunt resistances, along with a Lyot stop which acts as an aperture stop. A stable chassis design is shown using graphite-epoxy rods for long-term stability of radiance responsivity. The preamplifier gain ratios are measured for use over the five-decade dynamic range required of the radiation thermometer as the blackbody temperatures range from 150°C to 1,000°C. In addition to the use of this radiation thermometer as an ITS-90 transfer radiation thermometer, we outline a possible approach to directly measure thermodynamic temperature using an absolute detector-based radiance responsivity calibration.

References

1. T. Ricolfi, M. Battuello, F. Girard, G. Machin, H. McEvoy, S. Ugur, A. Diril, Meas. Sci. Technol. **13**, 2090 (2002)
2. F. Girard, T. Ricolfi, in *Proceedings TEMPMEKO 2004, 9th International Symposium on Temperature and Thermal Measurements in Industry and Science*, ed. by D. Zvizdić (FSB/LPM, Zagreb, Croatia, 2005), pp. 827–832
3. T. Ricolfi, F. Girard, in *Proceedings of TEMPMEKO '99, 7th International Symposium on Temperature and Thermal Measurements in Industry and Science*, ed. by J.F. Dubbeldam, M.J. de Groot (Edauw Johannissen bv, Delft, 1999), pp. 593–598
4. B. Gutschwager, S. Schiller, J. Hartmann, J. Hollandt, in *Proceedings TEMPMEKO 2004, 9th International Symposium on Temperature and Thermal Measurements in Industry and Science*, ed. by D. Zvizdić (FSB/LPM, Zagreb, Croatia, 2005), pp. 605–610
5. G. Romeo, G. Frulla, J. Compos. Mater. **29**, 751 (1995)
6. G.P. Eppeldauer, J. Res. Natl. Bur. Stand. (U.S.) **105**, 29 (2000)
7. H.W. Yoon, D.W. Allen, R.D. Saunders, Metrologia **42**, 89 (2005)
8. D.W. Allen, G. Dezsi, H.W. Yoon, in *Proceedings TEMPMEKO 2004, 9th International Symposium on Temperature and Thermal Measurements in Industry and Science*, ed. by D. Zvizdić (FSB/LPM, Zagreb, Croatia, 2005), pp. 817–822
9. H.W. Yoon, D.W. Allen, C.E. Gibson, M. Litorja, R.D. Saunders, S.W. Brown, G.P. Eppeldauer, K.R. Lykke, Appl. Optics **46**, 2870 (2007)
10. S.W. Brown, G.P. Eppeldauer, K.R. Lykke, Appl. Optics **45**, 8218 (2006)